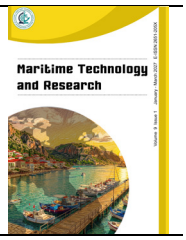
Maritime Technology and Research

https://so04.tci-thaijo.org/index.php/MTR



Research Article

Hydraulic stability of interlocking modular hexagonal artificial reefs under varying water levels

Haryo Dwito Armono[1,*], Suwardi[2], Dendy Satrio[1], Wahyudi[1] and Ahmad Qaedi Luthfi[1]

[1]*Department of Ocean Engineering, Sepuluh Nopember Institute of Technology, Indonesia*
[2]*Denpasar Marine Management Center, Ministry of Marine Affairs and Fisheries, Indonesia*

[*]*Corresponding author's e-mail address: armono@its.ac.id*

Article information

Received: May 28, 2026
Revision: August 17, 2026
Accepted: September 23, 2026

Keywords
Artificial reef;
Hydraulic stability;
Interlocking;
Modular reef;
Physical model test

Abstract

Artificial reefs are increasingly used as submerged coastal protection structures. However, their performance may be compromised when individual units slide, roll, scatter, or progressively displace under wave loads. Although geometric interlocking is often assumed to enhance modular reef stability, its influence on stability response under varying water levels and wave conditions remains insufficiently quantified. This study experimentally evaluates the hydraulic stability of new Interlocking Modular Hexagonal Artificial Reefs (IMHAR) using physical model tests in a wave flume. The interlocking and non-interlocking arrays are tested at a 1:15 Froude scale using seven multilayer configurations, three water levels (Low Water Spring (LWS), Mean Sea Level (MSL), and High Water Spring (HWS)), and three paired significant wave height and period cases. Stability is assessed using visual unit-state classification, percentage stability and damage, interlocking-induced stability gain, and a dimensionless stability number framework. The results show that interlocking units consistently improves stability, particularly under high-wave and low-water conditions. Under the LWS in the highest wave case, the interlocking arrays retain 50.0 - 86.4 % stability, whereas the non-interlocking arrays decrease to 20.0 - 53.0 %. The 731-GR (seven-base pointy-side) group configuration shows the most robust response among the tested layouts, whereas the 631-SL (six-base flat-side) single configuration is the most vulnerable. These findings indicate that, under the tested laboratory conditions, interlocking acts not only as a geometric modification but also as a collective stability mechanism that preserves array compactness and delays unit mobilization. This study provides a stability-oriented experimental basis for designing the placement of modular submerged artificial reefs for coastal protection.

Nomenclature

Symbol / Term	Definition
Dn	Nominal characteristic size of reef unit, calculated from measured unit volume
g	Gravitational acceleration
Hs	Measured significant wave height ($H_{1/3}$)
HWS	High Water Spring
IMHAR	Interlocking Modular Hexagonal Artificial Reef
LWS	Low Water Spring
MSL	Mean Sea Level
Nf	Number of damaged/failed reef units (Nsl + Nro + Nsc)
Nro	Number of rolling reef units
Ns	Dimensionless stability number
Nsc	Number of scattered reef units
Nsl	Number of sliding reef units
Nst	Number of stable reef units
Nt	Total number of reef units
Pdm	Percentage of damaged/failed units
Pst	Percentage of stable units
Tp	Measured peak period
USI	Optional unit-state severity index
V	Measured unit volume
Δ	Relative submerged density (ρs/ρw – 1)
ΔPst	Absolute stability gains due to interlocking (%)
ε	Dimensionless wave-steepness parameter
ρs	Reef-unit material density
ρw	Water density

1. Introduction

Artificial reefs are increasingly used as multifunctional coastal structures that combine ecological enhancement and engineering functions (Suwardi et al., 2026). In shallow-marine environments, artificial reefs can provide hard substrates, increase habitat complexity, modify local hydrodynamics, and reduce wave energy when their geometry and placement are properly designed (Ghiasian et al., 2021; Kuang et al., 2020; Ramm et al., 2021). Recent studies on porous, modular, and nature-inclusive reef systems have further demonstrated their potential for coastal protection and shoreline resilience through wave transformation, wave energy dissipation, and the creation of potentially ecologically compatible hard substrate systems (Dinu et al., 2025; Huang et al., 2024, 2025; Norris et al., 2025; Peng et al., 2024). However, these expected ecological and engineering benefits depend on the reef system's ability to maintain hydraulic stability under repeated wave loading.

Hydraulic instability can compromise the protective and ecological functions of artificial reefs. A modular reef array that experiences sliding, rolling, scattering, or substantial displacement

may lose its intended geometry and no longer behave as a functional, submerged coastal structure. This problem is more complex for modular reefs than for monolithic submerged structures because modular-reef stability depends not only on the weight, shape, and density of individual units but also on inter-unit contact, layout geometry, and the degree of mechanical continuity within the array. Under increasingly severe wave conditions, local displacement of a single unit may disturb adjacent units, weaken inter-unit contact, and destabilize the surrounding array.

Displacement-based stability assessment is widely used for coastal structures in which hydraulic instability may be expressed through deformation, displacement, or loss of the intended structural arrangement rather than through complete collapse alone. For submerged and low-crested modular structures, these observable unit responses provide a practical basis for evaluating hydraulic stability (Dassanayake & Oumeraci, 2012; Elias et al., 2021; Recio & Oumeraci, 2007, 2009). Similar reasoning applies to modular artificial reefs, where functional loss may occur through unit displacement, loss of contact, or disruption of array compactness. For hexagonal artificial reefs, Hanif and Armono (2022) used percentage damage to evaluate non-interlocking reef arrangements. Nevertheless, the stability response of mechanically interlocked multilayer reef arrays remains insufficiently quantified, particularly across different wave conditions and water levels.

A key unresolved issue is whether geometric interlocking alters the failure mechanism of modular reef systems. In non-interlocking arrays, individual units tend to resist hydrodynamic loading independently; once the local resistance is exceeded, sliding or rolling may propagate through the arrangement. In contrast, an interlocking mechanism is expected to restrict the relative movement among adjacent units, preserve array compactness, and promote collective resistance. This expected benefit is often discussed conceptually; however, systematic experimental evidence under varying water levels and wave conditions remains limited. Consequently, design guidance for modular artificial reefs still lacks sufficient stability-oriented evidence regarding how mechanical connectivity affects stability responses.

The water level adds further complexity because relative submergence controls the zone and intensity of wave-structure interaction. A reef that appears stable under mean or high water may become more vulnerable under lower water levels, where the upper units are more directly exposed to wave-induced mobilization. Conversely, increased submergence may reduce direct unit displacement, but may not fully compensate for the absence of a mechanical connection in non-interlocking systems. Therefore, the stability assessment of modular submerged reefs should consider wave conditions, water level, and interlocking and configuration geometry together rather than treating these parameters independently.

This study experimentally evaluated the hydraulic stability of the new Interlocking Modular Hexagonal Artificial Reef (IMHAR), a modified hexagonal artificial reef (Armono & Wirayuhanto, 2018), using wave flume physical model tests. The previous conventional hexagonal artificial reef unit represents a non-interlocking system in which individual units are stacked or arranged without mechanical interlocking, as shown in **Figure 1**.

The IMHAR unit introduces a crown-like locking element at the upper part of the module, allowing adjacent and vertically stacked units to engage mechanically to resist lateral movement. This modification was intended to reduce the relative movement among units and improve the collective stability of the multilayer reef array under wave loading. The final crown-lock geometry in IMHAR was selected previously through an iterative design process. Three interlocking alternatives were evaluated: truncated-cone, trapezoidal, and parallelogram-based crown-lock geometries. The truncated-cone and trapezoidal alternatives produced only partial engagement as the multilayer arrangement became more complex. In contrast, the crown-lock geometry provided the most

consistent inter-unit engagement through the three-layer assembly while remaining compatible with the modular hexagonal form. On this basis, the crown-lock configuration was selected as the final design for the hydraulic-stability experiments.

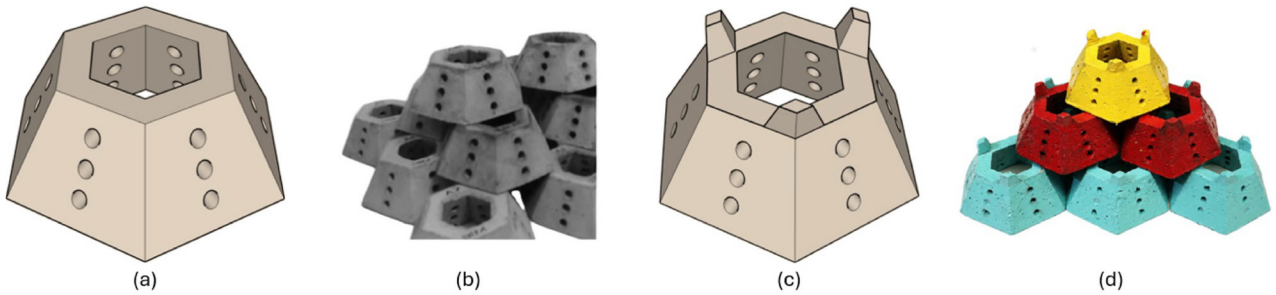


Figure 1 Development of hexagonal artificial reef unit: (a) conventional hexagonal artificial reef design, (b) conventional hexagonal artificial reef stacks, (c) IMHAR design, and (d) three-layer IMHAR stacks.

The analysis in this study is intentionally stability-oriented and does not interpret the observed unit states as a temporal damage sequence. The objectives were to (1) compare interlocking and non-interlocking reef arrays, (2) evaluate the influence of prescribed wave conditions and water level on the stability response, (3) identify the most and least stable configurations within the tested matrix, and (4) interpret the observed unit states using percentage stability, percentage damage, interlocking-induced stability gain, and a supporting dimensionless stability-number framework.

2. Materials and methods

2.1 Experimental design

A laboratory physical-model approach was used to evaluate the stability of interlocking and non-interlocking modular hexagonal artificial reef arrays under controlled wave loadings. The experiment focused on three main factors: mechanical connectivity, reef-array configuration, and hydraulic conditions. Mechanical connectivity was represented by interlocking and non-interlocking systems. The reef-array configuration was represented by different multilayer layouts and wave-facing orientations. Hydraulic conditions were represented by prescribed paired wave conditions and water level variations. The hydraulic stability was evaluated using visual unit-state classification, percentage stability, percentage damage, interlocking-induced stability gain, and a supporting dimensionless stability-number framework. This focused scope maintained a clear link between experimental observations and the proposed stability mechanism.

2.2 Physical model and similarity

The IMHAR model, developed from a conventional hexagonal artificial reef concept (Armono & Wirayuhanto, 2018), was physically tested in the wave flume to assess its stability. The main structural elements of the IMHAR are shown in **Figure 2**. The hexagonal shape provides repeated modularity and allows the units to be arranged in multilayer configurations. The interlocking element is the key distinction between the IMHAR and a previous conventional hexagonal artificial reef, as it restricts relative displacement among adjacent units. The modular component concept supports a flexible arrangement, whereas the perforated sidewalls provide porosity and prevent the reef from behaving as a fully solid block.

This Froude-scaling approach was selected because the stability problem is governed primarily by gravity-dominated wave-structure interaction. Froude-based physical modeling is widely used in coastal engineering experiments when gravity and inertia dominate the governing response, provided that scale effects and model limitations are clearly acknowledged (CIRIA et al.,

2007; Eldrup et al., 2019; Hughes, 1993). The experiments were conducted at a geometric scale of 1:15 based on Froude similarity. This scaling ratio was selected to preserve the relative balance between inertial and gravitational effects while keeping the physical model compatible with the available flume dimensions and wave-generation capacity.

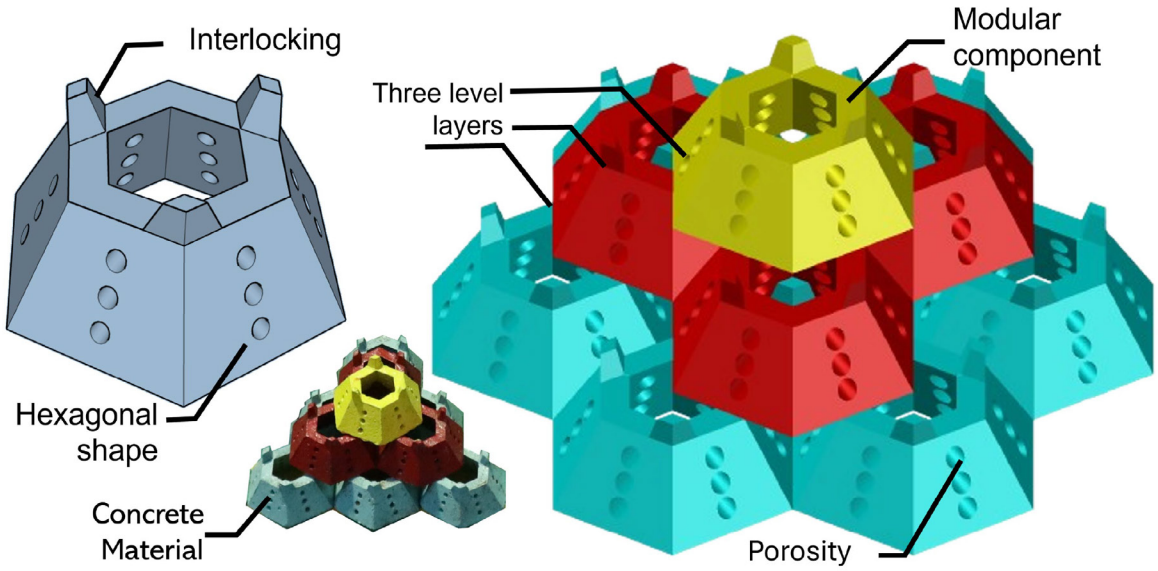


Figure 2 Key structural elements of IMHAR system.

The final laboratory-scale model unit had an overall outer width of 250 mm and a body height of 100 mm, with a 90-mm central hexagonal opening. Circular side openings with a diameter of 6 mm were incorporated into the inclined faces. The interlocking (IMHAR) variant incorporated the crown-lock feature, whereas the non-interlocking variant retained the same basic geometry, dimensions, porosity, material, and placement configuration without mechanical locking. **Figure 3** shows the IMHAR model dimensions.

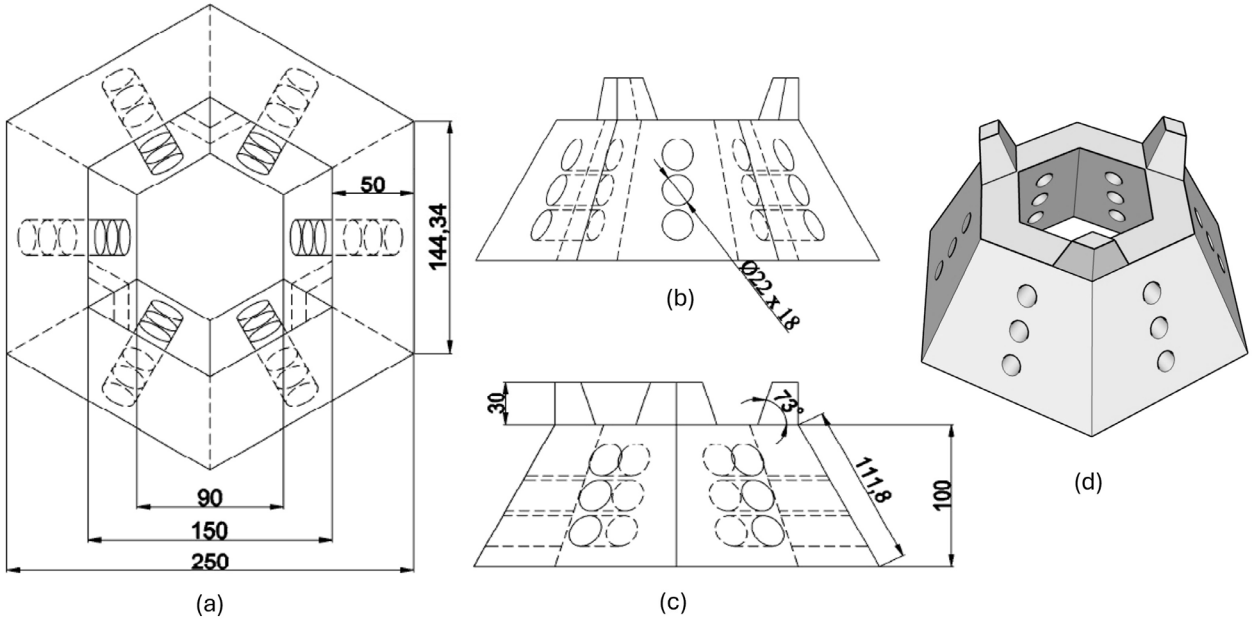


Figure 3 IMHAR model dimensions: (a) top view, (b) side view, (c) front view, and (d) 3D view.

The laboratory-scale IMHAR model units were fabricated using a 3D-printed master and mould-casting procedure. The final geometry was first reproduced as a polylactic acid (PLA) physical master using 3D printing, which served as the dimensional reference for fabricating a reusable 0.8-mm steel-plate mould. The model units were cast using a cement–fine aggregate mixture of approximately 2:1, with water added gradually to obtain sufficient workability for the detailed mold geometry. Light controlled compaction was applied during casting to reduce entrapped air. After demolding, all units were visually and dimensionally inspected, weighed, and color-coded according to their initial layer positions before hydraulic testing. The same fabrication procedure was applied to all model units tested in the laboratory. The average weight of a single model unit was 305.51 g for the interlocking units and 274.59 g for the non-interlocking units.

2.3 Wave flume setup

The experiments were conducted in a 20-m-long, 2.3-m-wide, and 2.5-m-high wave flume equipped with an automated plunger-type wave generator capable of generating regular and irregular waves with various wave spectra. The wave flume testing system also consisted of a sponge-type wave absorber, five wave probes, and a sloping bed in front of the model testing placement zone. The sponge-type wave absorber was installed at the end of the flume to reduce reflected-wave effects. The wave probes monitored and recorded free-surface variations, which were processed using a zero-crossing procedure to obtain significant wave height (Hs) and peak period (Tp) of the prescribed wave spectrum. No dedicated incident-reflected wave-separation procedure was applied because wave reflection was not treated as a response variable that influenced stability.

As shown in **Figure 4**, the IMHAR model was positioned approximately 14 m from the wave generator. A sloping sandy seabed was constructed using an approximately 15-cm-thick sand layer, with a 1:22 nearshore slope transitioning to a 1:5 offshore slope because of the available flume length. The median sand layer grain diameter of 0.215 mm was not scaled; therefore, it should not be interpreted as a movable-bed model of scour or sediment transport. Fine sand was placed on the bed to reduce IMHAR bottom-layer slip during testing. A load cell was also installed to record the wave-induced load on the structure; detailed force-distribution analysis will be discussed in another paper and is outside the scope of this stability-focused paper.

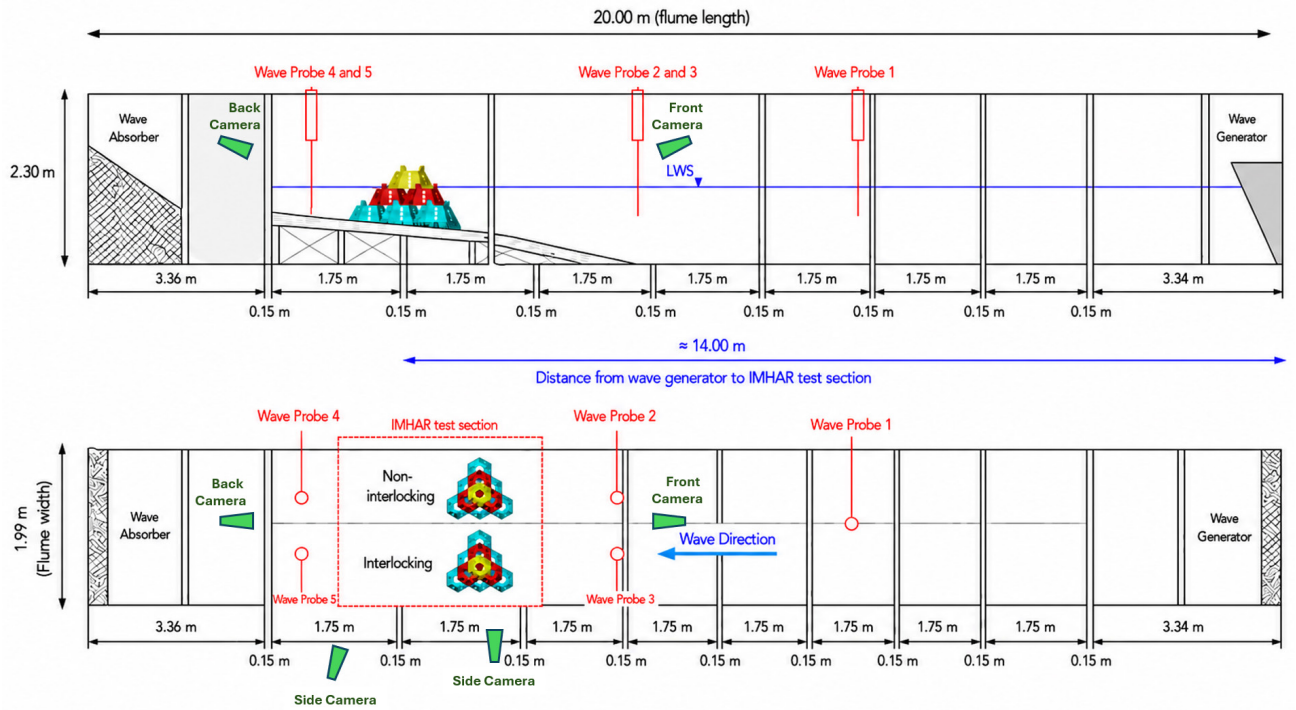


Figure 4 IMHAR experimental setup: (a) side view and (b) top view of wave flume.

While the probes monitored the water-surface response and the load cell recorded the incoming wave force, four CCTV cameras captured and documented hexagonal artificial unit movement and post-test damage from multiple viewing angles, as shown in **Figure 4**. The paired camera placement enabled the comparison of interlocking and non-interlocking arrays under comparable hydraulic conditions. **Figure 5** shows typical recordings from four CCTV cameras taken before the experiment.



Figure 5 Typical CCTV recording of experimental setup and instrument layout in the wave flume before testing.

2.4 Reef configurations and hydraulic conditions

Seven multilayer reef configurations were tested to represent variations in layer composition, array grouping, and incident-wave orientation, as shown in **Figure 6**. The numerical codes 6-3-1 and 7-3-1 indicate the number of reef units in the bottom, middle, and top layers. The letters S and G denote single and group arrangements, and L and R denote flat-side and pointy-side facing the normally incident wave direction. **Table 1** lists the IMHAR configuration in this study.

Table 1 IMHAR configuration types, arrays, and tested units.

Type	Variation	Number of Arrays	Number of Unit
631-SL	10 unit single with flat-side orientation	1	10
631-SR	10 unit single with pointy-side orientation	1	10
631-GL	60-unit group with flat-side orientation	6	60
631-GR	60 unit group with pointy-side orientation	6	60
731-S	11 unit single with any-side orientation	1	11
731-GL	66 unit group with flat-side orientation	6	66
731-GR	66 unit group with pointy-side orientation	6	66
Total		**27**	**283**

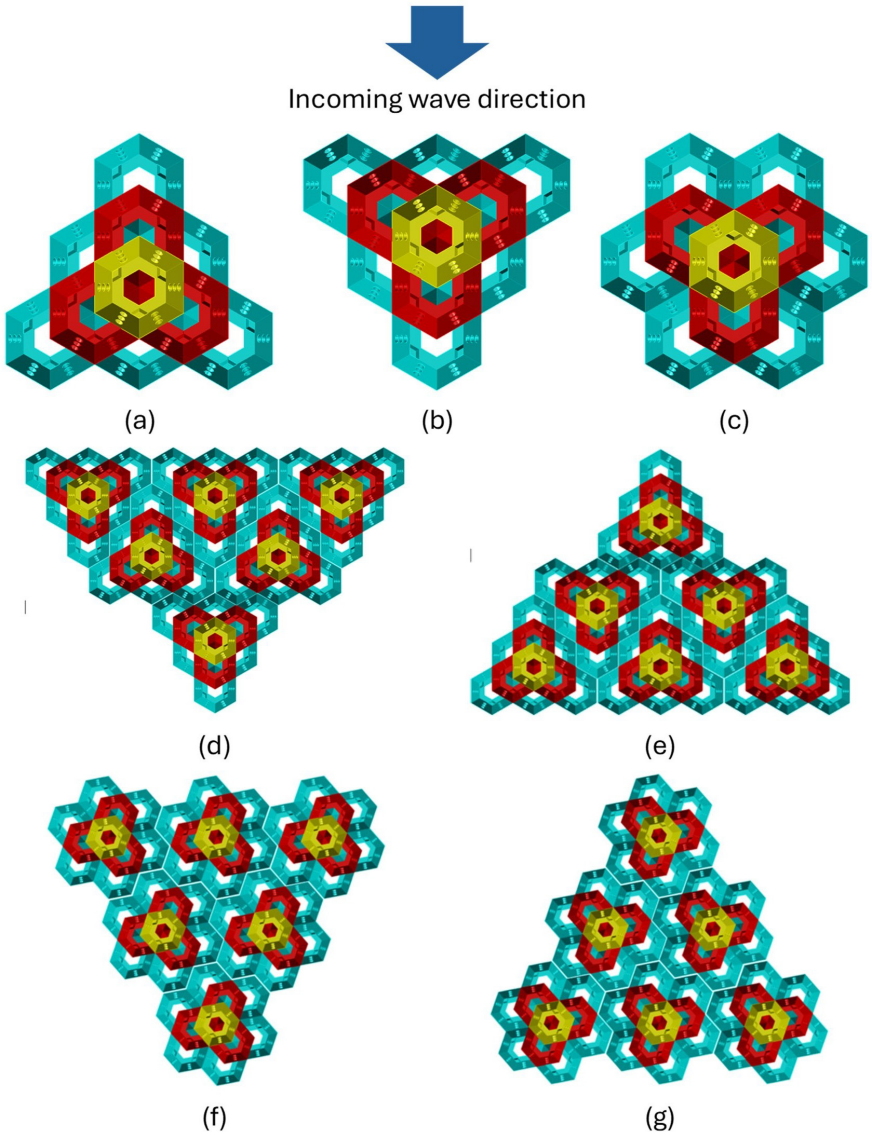


Figure 6 Hexagonal artificial reef configuration variations: (a) 631-SR, (b) 631-SL, (c) 731-S, (d) 631-GL, (e) 631-GR, (f) 731-GL, and (g) 731-GR.

The hydraulic experimental matrix consisted of three water levels, LWS = 75 cm, MSL = 79.5 cm, and HWS = 84 cm, and three prescribed irregular-wave conditions generated using a JONSWAP spectrum with $\gamma = 3.3$. The nominal H5, H10, and H15 conditions corresponded to significant wave heights of 5, 10, and 15 cm paired with significant wave periods of 1.0, 1.2, and 1.4 s, respectively. Wave height and period were therefore prescribed as paired hydraulic conditions rather than independently varied factors. Seven reef configurations were combined with three wave conditions and three water levels, resulting in 63 experimental scenarios. **Table 2** presents the experimental matrix for the physical model tests.

For each scenario, the corresponding interlocking (IL) and non-interlocking (NIL) arrays were positioned side by side in the flume and tested simultaneously under the same incident-wave condition; consequently, the paired IL-NIL comparison did not double the number of scenarios to 126. Each scenario consisted of a single 30-min run. The prescribed wave conditions were tested sequentially from H5 to H10 and H15. After every run, the final unit condition was documented, all reef units were returned to their initial positions, and the sandy seabed was restored before the subsequent test. Accordingly, each run was treated as an independent final-state assessment rather than as cumulative damage from the preceding wave condition.

Table 2 Experimental matrix for IMHAR hydraulic stability tests.

Parameter	Variation
Reef system	Interlocking; non-interlocking
Configuration	631-SR; 631-SL; 731-S; 631-GL; 631-GR; 731-GL; 731-GR
Water depth (cm)	75 cm (LWS); 79.5 cm (MSL); 84 cm (HWS)
Wave height case (cm)	5 cm; 10 cm; 15 cm (H5, H10, H15)
Model-scale period (second)	1.0 s; 1.2 s; 1.4 s
Scale	1:15 Froude scale
Test duration	30 min per scenario
Primary response	Damage state and percentage stability

2.5 Damage-state classification

Hydraulic stability was assessed using an operational displacement-based damage classification with four states: stable, sliding, rolling, and scattered states, as shown in **Figure 7**. A unit was classified as stable when its horizontal displacement was less than half of the upper flat-side width, or its vertical lifting was less than half of the locking element height. Sliding indicated horizontal displacement beyond this threshold, whereas the unit remained upright and generally within the array. Rolling indicated a clear rotational movement or loss of the original upright orientation while the unit remained near the initial array. Scattered indicated detachment from the functional array and loss of contact or proximity to the original position.

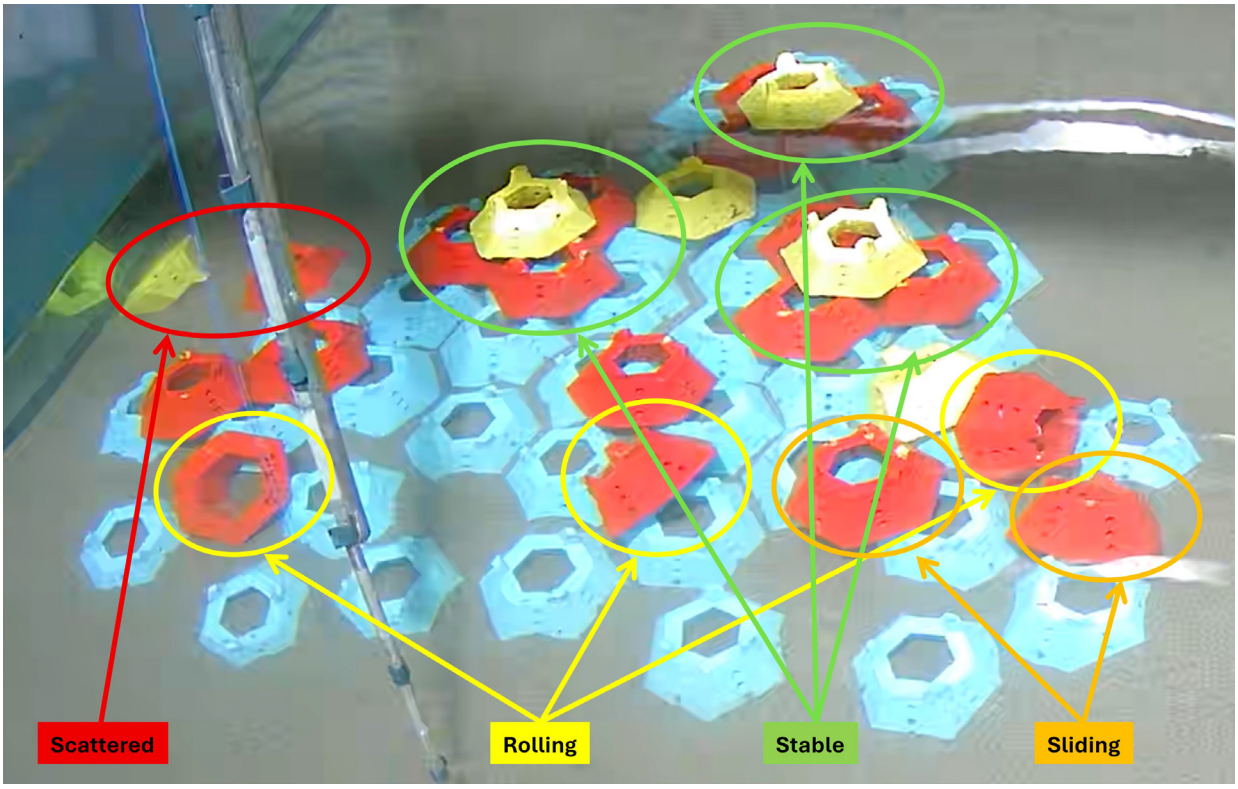


Figure 7 Unit-state classification of hexagonal artificial reef arrays in wave flume.

Figure 7 illustrates the four conditions of observed IMHAR units used for the stability assessment. Only stable units were counted as stable responses, whereas sliding, rolling, and scattered units were grouped as unstable responses, as listed in **Table 3**. The distinction among these states was

retained to describe the observed mode of instability rather than to imply a temporal sequence of damage. The IMHAR model stability states were verified through direct observation and CCTV recordings. The models were color-coded by initial layer position to facilitate tracking: green for the bottom layer, red for the middle layer, and yellow for the upper layer.

Table 3 Unit-state classification used for hydraulic stability assessment.

Damage state	Operational criterion	Mechanical interpretation	Quantitative treatment
Stable	Displacement below the defined threshold	No functional loss of array position	Stable unit
Sliding	Translation beyond threshold; unit remains upright	Translational mobilization without rotational failure	Unstable response, Damaged/ failed unit
Rolling	Tilting, rolling, overturned, or loss of original orientation	Rotational instability and partial loss of support	Unstable response, Damaged/ failed unit
Scattered	Detachment from the functional array	Complete local detachment from the arrangement	Unstable response, Damaged/ failed unit

2.6 Stability metrics and data analysis

For each test, the total number of reef units was denoted as *Nt*, the number of stable units as *Nst*, and the number of damaged or failed units as *Nf*, respectively. The damaged or failed units were classified as sliding, rolling, or scattered. Therefore, the total number of failed units is expressed as:

$$N_f = N_{sl} + N_{ro} + N_{sc} \quad (1)$$

where *Nsl*, *Nro*, and *Nsc* are the numbers of sliding, rolling, and scattered units, respectively. The percentage stability and damage were calculated as follows:

$$Pst = \frac{N_{st}}{N_t} \times 100 \quad (2)$$

$$Pdm = \frac{N_f}{N_t} \times 100 = 100 - Pst \quad (3)$$

where Pst is the percentage of stable units, and Pdm is the percentage of damaged or failed units after wave loading.

The absolute stability gain owing to interlocking was calculated by comparing paired interlocking and non-interlocking arrays under the same configuration and hydraulic conditions:

$$\Delta Pst = Pst_{IL} - Pst_{NIL} \quad (4)$$

where Pst_{IL} and Pst_{NIL} are the stability percentages of the paired interlocking and non-interlocking arrays, respectively. ΔPst is reported in percentages, with positive values indicating improved stability owing to interlocking.

Where detailed damage mode counts are available, a unit-state severity index can be calculated as:

$$USI = \frac{(1 \times N_{sl}) + (2 \times N_{ro}) + (3 \times N_{sc})}{3N_t} \times 100 \quad (5)$$

The primary analysis emphasized percentage stability and percentage damage because these metrics were consistently available across all tested conditions. The unit-state severity index was retained only as an optional descriptive formulation and was not used as a primary response metric in the present results.

The dimensionless stability number is defined as:

$$N_s = \frac{Hs}{\Delta D_n} \quad (6)$$

where Hs is the measured significant wave height ($H_{1/3}$), *Dn* is the nominal characteristic size of the reef unit, and Δ is the relative submerged density. The relative submerged density was calculated as follows:

$$\Delta = \frac{\rho_s}{\rho_w} - 1 \quad (7)$$

where ρs and ρw are the reef unit material density and water density, respectively. The nominal characteristic size, *Dn* , was estimated from the measured unit volume as follows:

$$D_n = V^{1/3} \quad (8)$$

The representative measured volumes of IMHAR (interlocking) and non-interlocking hexagonal reef units in this study were 206 and 184 mL, respectively.

The dimensionless wave-steepness parameter (ε) was defined as:

$$\varepsilon = \frac{Hs}{gT_p^2} \quad (9)$$

where Hs is the significant wave height, g is the gravitational acceleration, and Tp is the peak period of the incoming waves

In this study, the stability-number response is interpreted alongside percentage stability and the observed unit state. For the non-interlocking system, the resistance characterization was based on the average mass of an individual mechanically independent unit. For IMHAR (the interlocking system), the adopted group-stability formulation used the cumulative measured mass of the mechanically engaged units in the corresponding configuration. Because the two formulations represent different mechanical resistance scales, the resulting Ns values are used only as supporting system-level indicators within the adopted framework and are not interpreted as directly transferable universal single-unit stability thresholds. The primary evidence for the effect of interlocking remains the paired observed unit states and percentage-stability response. Each hydraulic scenario was tested

once; therefore, inter-run standard deviation, confidence intervals, and statistical repeatability could not be quantified.

3. Results

3.1 Consolidated quantitative evidence

Table 4 lists the results of quantitative indicators' stability. The overall mean stability was calculated across the complete experimental matrix for each reef system. Mean stability at H5, H10, and H15 was calculated across all seven configurations and all three water levels for the corresponding prescribed wave condition, whereas mean stability at the LWS, MSL, and HWS was calculated across all seven configurations and all three prescribed wave conditions for the corresponding water level. Across all tested scenarios, the interlocking arrays achieved a mean stability of 95.5 %, whereas the non-interlocking arrays achieved 72.8 %. This 22.7 % difference reflects the observed system-level stability contrast within the present experimental matrix.

Table 4 Consolidated quantitative indicators for stability analysis.

Indicator	Interlocking	Non-interlocking	Main interpretation
Overall mean stability	95.5 %	72.8 %	Higher observed system-level stability for the interlocking arrays within the tested matrix.
Mean stability at H5	100.0 %	95.0 %	The difference was small under mild waves.
Mean stability at H10	100.0 %	71.6 %	The non-interlocking arrays began to degrade.
Mean stability at H15	86.4 %	51.8 %	The largest wave-condition contrast occurred under H15.
Mean stability at LWS	90.1 %	62.4 %	LWS produced the lowest mean stability within the tested water levels.
Mean stability at MSL	96.5 %	76.1 %	The stability improved with increasing water level.
Mean stability at HWS	99.8 %	79.9 %	The interlocking arrays remained near-complete stability at HWS.
Stability range at LWS-H15	50.0 - 86.4 %	20.0 - 53.0 %	Largest stability contrast within the tested LWS-H15 condition.
Best-performing configuration	731-GR, mean 97.7 %	731-GR, mean 79.8 %	Most robust tested layout.
Weakest configuration	631-SL, mean 92.2 %	631-SL, mean 62.2 %	Most vulnerable tested layout.
Largest paired stability gain	+60 % points	-	Observed for 631-SL under HWS-H15.

The stability gain was not uniform across the prescribed hydraulic conditions. Under the mild wave condition (H5), both systems remained mostly stable; therefore, the additional contribution of interlocking was relatively small. As hydraulic severity increased from H5 to H15, the non-interlocking arrays exhibited substantially greater unit mobilization, whereas the interlocking arrays maintained higher stability. Because wave height and significant period were paired in the experimental matrix, this trend is interpreted as a response to increasing prescribed hydraulic severity rather than as an isolated wave height effect.

3.2 Effect of interlocking and wave height

The effect of interlocking became increasingly visible as wave height increased. At H5, the interlocking and non-interlocking arrays had mean stability values of 100.0 and 95.0 %, respectively, resulting in a modest stability gain of 5.0 %. At H10, the mean stability of the non-interlocking arrays decreased to 71.6 %, whereas all interlocking arrays remained fully stable, increasing the stability gain to 28.4 %. At H15, the non-interlocking arrays decreased further to 51.8 %, whereas the interlocking arrays remained at 86.4 % mean stability, resulting in a gain of 34.6 %. **Tables 5 - 7** below show the stability of the hexagonal reef configuration under all water-level and wave conditions.

Table 5 Stability comparison of hexagonal artificial reef arrays at H5 cm (low wave condition).

No	Type	Interlocking			Non-interlocking		
		LWS	MSL	HWS	LWS	MSL	HWS
1	631-SL	100 %	100 %	100 %	90 %	100 %	90 %
2	631-SR	100 %	100 %	100 %	90 %	100 %	100 %
3	731-S	100 %	100 %	100 %	91 %	100 %	100 %
4	631-GL	100 %	100 %	100 %	87 %	100 %	95 %
5	631-GR	100 %	100 %	100 %	90 %	100 %	97 %
6	731-GL	100 %	100 %	100 %	83 %	100 %	94 %
7	731-GR	100 %	100 %	100 %	92 %	100 %	97 %

Table 6 Stability comparison of hexagonal artificial reef arrays at H10 cm (moderate wave condition).

No	Type	Interlocking			Non-interlocking		
		LWS	MSL	HWS	LWS	MSL	HWS
1	631-SL	100 %	100 %	100 %	50 %	60 %	70 %
2	631-SR	100 %	100 %	100 %	60 %	70 %	80 %
3	731-S	100 %	100 %	100 %	64 %	82 %	82 %
4	631-GL	100 %	100 %	100 %	50 %	70 %	90 %
5	631-GR	100 %	100 %	100 %	58 %	73 %	93 %
6	731-GL	100 %	100 %	100 %	53 %	73 %	85 %
7	731-GR	100 %	100 %	100 %	70 %	77 %	94 %

Table 7 Stability comparison of hexagonal artificial reef arrays at H15 cm (extreme wave condition).

No	Type	Interlocking			Non-interlocking		
		LWS	MSL	HWS	LWS	MSL	HWS
1	631-SL	50 %	80 %	100 %	20 %	40 %	40 %
2	631-SR	70 %	90 %	100 %	30 %	60 %	50 %
3	731-S	55 %	91 %	100 %	45 %	64 %	64 %
4	631-GL	73 %	87 %	100 %	43 %	52 %	60 %
5	631-GR	82 %	92 %	97 %	47 %	57 %	63 %
6	731-GL	77 %	92 %	100 %	45 %	55 %	64 %
7	731-GR	86 %	95 %	98 %	53 %	65 %	70 %

The stability values in **Tables 5 - 7** show that the difference between the interlocking and non-interlocking systems became more pronounced as the wave loading increased. Under H5, all interlocking configurations remained 100 % stable across the LWS, MSL, and HWS. The non-interlocking configurations also exhibited relatively high stability, ranging from 83 to 100 %, indicating that the individual-unit resistance was generally sufficient under mild wave loading.

Under H10, all interlocking configurations maintained 100 % stability across the three water levels. In contrast, the non-interlocking configurations showed clear degradation, particularly at the LWS, where stability ranged from 50 to 70 %. Under H15, the contrast becomes stronger. Although the interlocking configurations showed reduced stability under LWS, with values ranging from 50 to 86 %, they remained more stable than the non-interlocking configurations under the same conditions. The non-interlocking arrays exhibited substantial instability, particularly at LWS, where stability fell to 20 - 53 %. Within the tested matrix, these observations indicate that mechanical interlocking increasingly restricted relative unit mobilization as the prescribed hydraulic severity increased.

3.3 Effect of water level

The water level exerted strong control on the stability response of the interlocking reef arrays. Under the LWS, the mean stability of the interlocking arrays was 90.1 %, whereas the non-interlocking arrays reached only 62.4 %. At the MSL, the corresponding values increased to 96.5 and 76.1 %. At the HWS, the interlocking arrays approached near-complete stability at 99.8 %, whereas the non-interlocking arrays reached 79.9 %. These results indicate that increasing water levels generally reduced the severity of unit mobilization, although the improvement was more pronounced in the interlocking system.

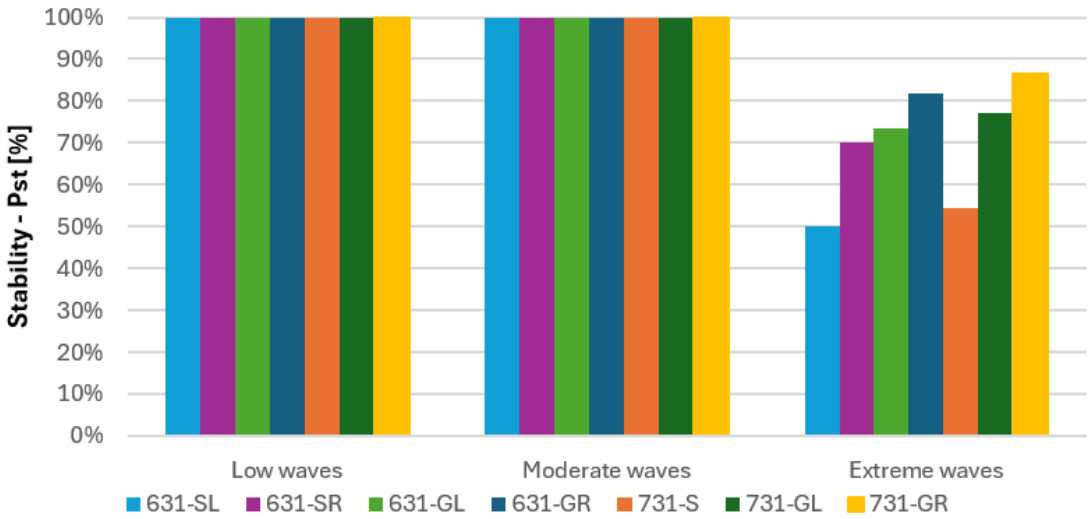


Figure 8 Stability percentage (Pst) of interlocking configurations under prescribed irregular-wave conditions at LWS.

As shown in **Figures 9** and **10**, the interlocking configurations remained essentially stable through H5 and H10 at the LWS, while stability clearly decreased under the more severe H15 condition. Under the HWS, the interlocking configurations remained close to complete stability across the tested wave conditions. Within the present experimental matrix, this contrast indicates that the lower water level produces the more critical stability response, particularly when combined with H15. The interpretation is specific to the tested paired wave conditions and should not be generalized beyond the present experimental range.

3.4 Critical condition: LWS-H15

The combined LWS-H15 condition produced the strongest contrast between the interlocking and non-interlocking systems. Under these conditions, the stability of interlocking arrays ranged from 50.0 - 86.4 %, whereas that of non-interlocking arrays decreased to 20.0 - 53.0 %. This confirms that the low water level combined with high wave loading represented the most critical condition in the present stability assessment.

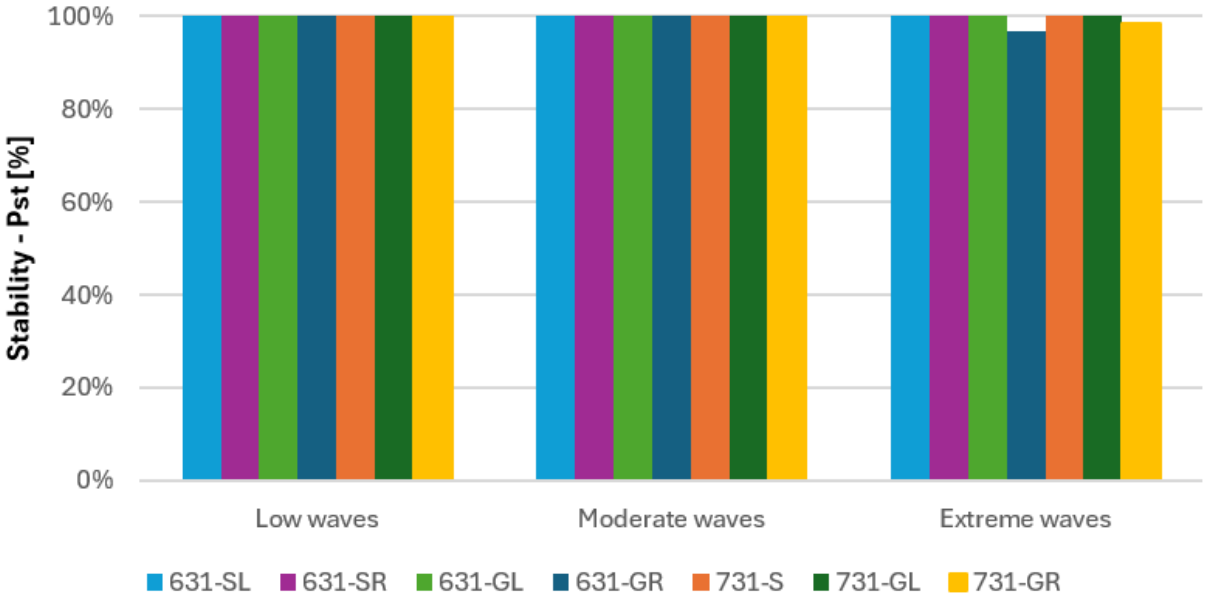


Figure 9 Stability percentage (Pst) of interlocking configurations under prescribed irregular-wave conditions at HWS.

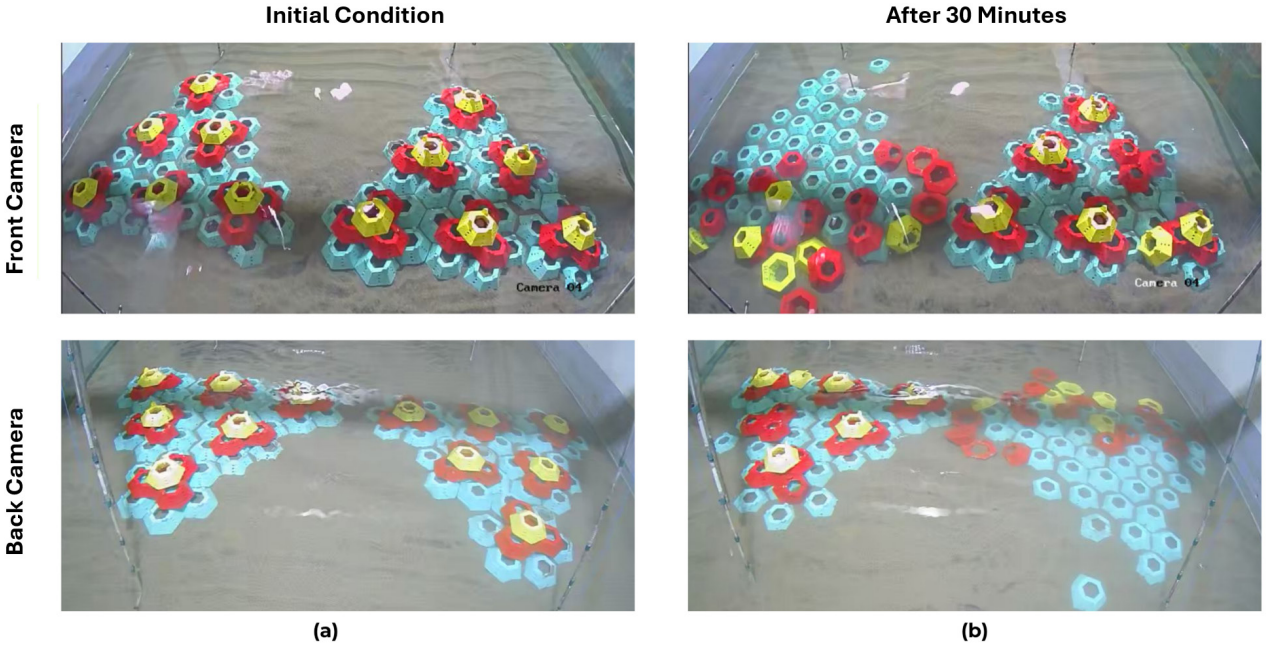


Figure 10 Stability response of 731-GR configuration (a) before and (b) after 30 minutes of 15 cm wave exposure under LWS conditions.

Figure 10 and the representative unit-state evidence in **Table 8** show that interlocking influenced both the magnitude and the observed mode of instability under LWS-H15. The non-interlocking arrays exhibited greater displacement, loss of compactness, and scattering of upper- and middle-layer units. In contrast, the interlocking arrays generally retained a more coherent arrangement, with instability remaining more localized when sliding or rolling occurred.

Table 8 Representative damage-mode evidence under LWS-H15 critical condition.

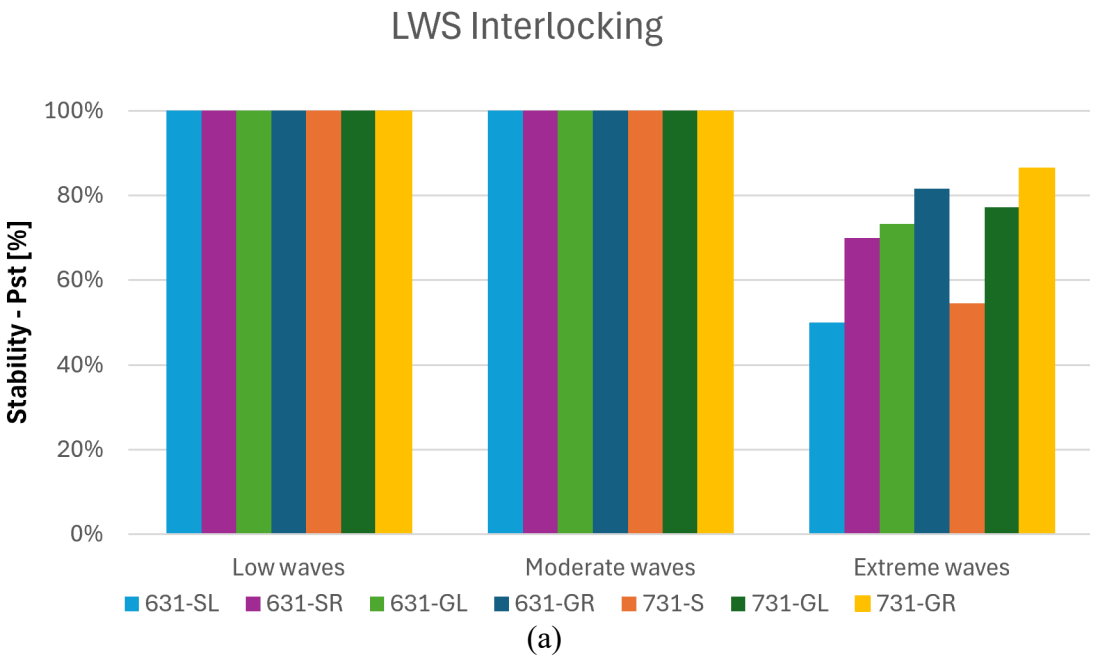
Configuration	System	Stable units	Main observed damage	Interpretation
631-SL	Interlocking	5/10	Mixed sliding and rolling, with scattering concentrated at the upper unit	Weakest interlocking layout; the effectiveness of the locking mechanism was limited and did not prevent damage under extreme loading
631-SL	Non-interlocking	2/10	Widespread sliding in the lower layer, rolling in the middle layer, and scattering at the upper layer	Instability affected almost the entire arrangement
731-GR	Interlocking	57/66	Localized damage mainly in the front-left group, while most units remained stable	Best-performing layout; the combined 7-3-1 grouped arrangement and pointy-side orientation was associated with the highest retained compactness
731-GR	Non-interlocking	35/66	Severe damage in the upper and middle layers, dominated by scattering and rolling	Loss of mechanical connectivity was associated with widespread instability across the array

The comparison indicates that interlocking shifted the failure response from widespread array disruption toward more localized unit mobilization. However, the 631-SL result also shows that interlocking alone was insufficient when the base geometry and wave-facing orientation are less favorable. Therefore, the critical LWS-H15 condition confirms that stability is governed by the combined effects of the mechanical connection, array geometry, and incident-wave orientation.

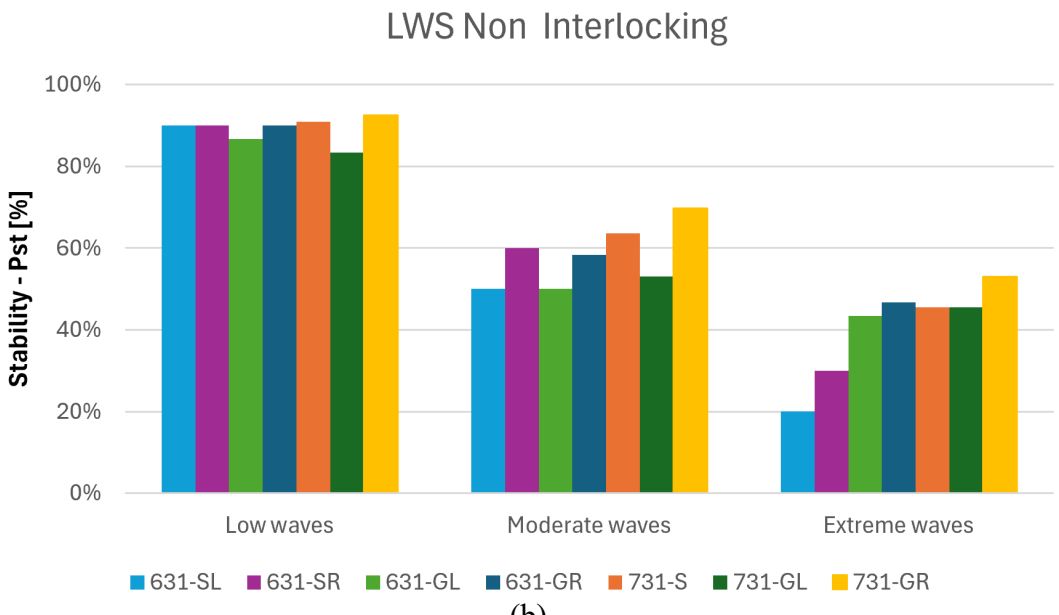
3.5 Configuration-dependent stability

The 731-GR configuration consistently exhibited the highest stability, with mean values of 97.7 and 79.8 % for the interlocking and non-interlocking systems, respectively. In contrast, 631-SL was the weakest configuration, with mean stability values of 92.2 and 62.2 % for the interlocking and non-interlocking systems, respectively.

Under LWS-H15, the interlocking 731-GR retained 86.4 % stability, whereas the non-interlocking 731-GR retained 53.0 %. In contrast, interlocking 631-SL retained only 50.0 %, and non-interlocking 631-SL decreased to 20.0 %. This comparison indicates that interlocking improves the observed stability within both configurations, while the baseline arrangement also influences the final response. Among the tested layouts, 731-GR combined the 7-3-1 layer arrangement, grouped placement, and pointy-side wave-facing orientation and produced the highest stability. Because these geometric factors were not varied independently in factorial design, their individual contributions cannot be isolated from the present dataset; the result should therefore be interpreted as a combined configuration effect.



(a)



(b)

Figure 11 Stability percentage (Pst) of (a) interlocking and (b) non-interlocking configurations under prescribed irregular-wave conditions at LWS.

Figures 8 and **11** present the measured stability percentages of the interlocking and non-interlocking configurations under the three prescribed irregular wave conditions at the LWS. The interlocking configurations remained at 100 % stability through H10 and then diverged under H15, while the group configurations generally retained higher stability levels. In contrast, the non-interlocking configurations had already declined by H10 and decreased further under H15. The plots are therefore interpreted as discrete experimental responses to the prescribed H5-H10-H15 conditions, with the connecting lines used only to aid visual comparison rather than to represent a fitted stability relationship. The weaker response of 631-SL and the stronger response of 731-GR further indicate that interlocking performance should be interpreted together with base arrangement, grouping, and wave-facing orientation.

3.6 Stability-number interpretation

The stability-number framework provides a supporting nondimensional description of the tested hydraulic conditions relative to the adopted resistance scale. In the present study, Ns was not used to derive a new critical stability threshold. Instead, the measured data were plotted against the wave-steepness parameter ε to examine how the nondimensional response varied across the three prescribed wave conditions within each configuration.

Figures 13 and **14** show an increasing Ns response with increasing wave steepness within both the interlocking and non-interlocking datasets under the LWS. The absolute magnitudes of Ns differ substantially between the two systems because the adopted resistance basis is different: the interlocking formulation represents the cumulative mechanically engaged group mass, whereas the non-interlocking formulation represents an individual independent unit. Therefore, the vertical separation between the two datasets should not be interpreted as a direct one-to-one measure of interlocking efficiency. Rather, the Ns plots are used as supporting system-level descriptors, while the paired percentage-stability and observed unit-state results provide the primary experimental evidence of the interlocking effect. This conservative interpretation is consistent with the limited number of wave conditions and the absence of repeated runs.

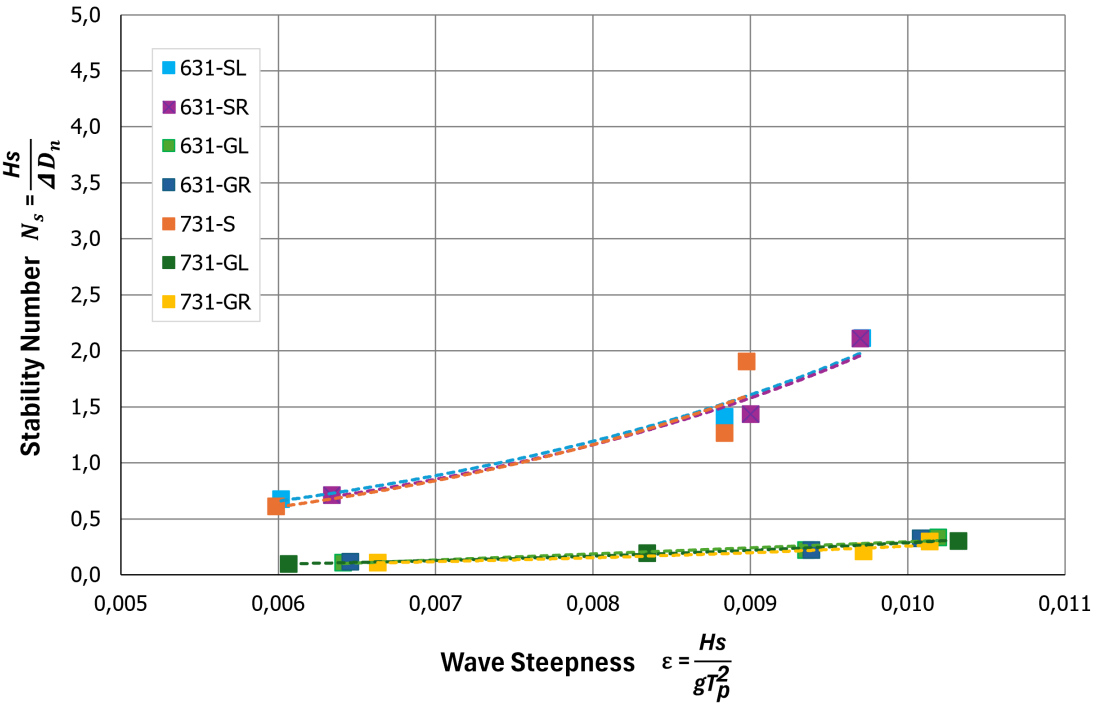


Figure 12 Relationship between stability number (Ns) and wave steepness (ε) under LWS conditions for interlocking configurations.

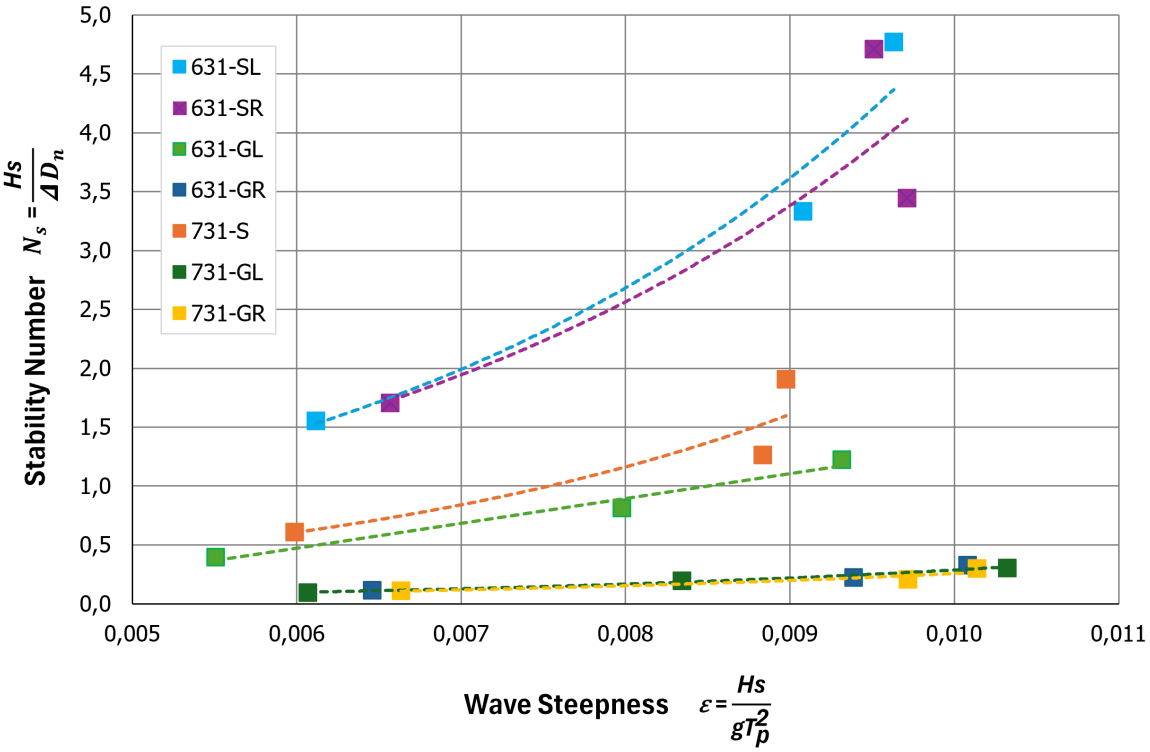


Figure 13 Relationship between stability number (Ns) and wave steepness (ε) under LWS conditions for non-interlocking configurations.

4. Discussion

4.1 Interlocking as a collective stability mechanism

The results show that interlocking modifies the stability mechanism from unit-scale resistance to system-scale resistance. In non-interlocking arrays, each unit resists wave loading primarily through its own submerged weight, geometry, and basal friction. Once the local resistance is exceeded, the mobilized unit can disturb the adjacent units and destabilize the surrounding arrangement. This mechanism is consistent with damage-based interpretations of modular and low-crested coastal structures, where the displacement of individual elements can reduce system integrity (Dassanayake & Oumeraci, 2012) .

In interlocking arrays, the locking element restricts relative displacement, increases the effective collective resistance, and allows part of the wave-induced demand to be redistributed through inter-unit contact. This explains why the additional benefit of interlocking was relatively small under H5 but became more evident under the more severe prescribed conditions. The LWS-H15 observations further indicate that interlocking did not simply increase the number of stable units; it also helped retain array compactness by limiting widespread scattering and more often confining instability to localized sliding or rolling.

This finding extends the previous work on hexagonal artificial reefs. Earlier studies have shown that hexagonal reef elements can serve as submerged modular structures and that the percentage of damage can be used to evaluate the stability of non-interlocking reefs (Armono et al., 2021; Hanif & Armono, 2022). The present study contributes to the stability-mechanism literature by demonstrating that mechanical connectivity improves the retention of structural integrity in multilayer modular reef arrays.

4.2 Influence of water level and configuration

The results identified the LWS as the governing condition for stability in the present experiments. Under the LWS, the reef crest and upper units were closer to the active wave-interaction zone, increasing the probability of direct unit mobilization. Increased submergence at the MSL and HWS improved stability, but non-interlocking arrays remained more vulnerable than interlocking arrays under high-wave loading. This conclusion is specific to the stability response evaluated in this study.

Configuration also influenced the measured stability. The 731-GR layout performed best, whereas the 631-SL layout performed worst. These results show that the locking mechanism should be considered together with the overall array geometry. The present matrix does not independently isolate the effects of base width, grouping, and wave-facing orientation; consequently, the superior response of 731-GR is interpreted as a combined configuration effect rather than as evidence that any one geometric factor alone controls stability. For practical deployment, unit geometry, mechanical connectivity, array layout, and governing hydraulic conditions should therefore be evaluated as coupled design variables.

From a design perspective, this configuration is important. If interlocking is applied to an unfavorable layout, stability may improve relative to the non-interlocking version; however, the final response may still be weaker than that of a more robust configuration. Therefore, the IMHAR design should be evaluated as an integrated system rather than as a single-unit modification.

4.3 Stability metrics and stability number

Unit-state classification and percentage stability provide a practical basis for evaluating modular reef stability because different displacement and orientation states represent different levels of structural disruption. In this study, sliding, rolling, and scattering were treated as failed states for percentage-stability calculation, whereas the distinctions among these states were retained to interpret the observed instability mode. Localized sliding or rolling may still leave part of the array compact, whereas scattering represents a more severe loss of the intended functional arrangement.

The stability-number response should be interpreted as a supporting nondimensional descriptor of the tested system rather than as a universal single-unit criterion. Within each dataset, Ns increased as wave steepness increased, reflecting the increasing hydraulic demand represented by the prescribed wave conditions. However, the absolute Ns magnitudes of the interlocking and non-interlocking systems should not be compared as equivalent single-unit quantities because the adopted resistance basis differs between the two formulations: cumulative mechanically engaged group mass for the interlocking system and individual-unit mass for the non-interlocking system. Accordingly, the Ns–ε plots complement, rather than replace, the paired percentage-stability and observed unit-state evidence.

This interpretation provides a more conservative basis for using the stability-number framework in the present study. The principal experimental conclusion is therefore derived from the paired stability percentages and observed unit states, while Ns is retained only to describe the nondimensional hydraulic-resistance response within the adopted formulations. Generalized critical Ns thresholds for IMHAR are not proposed from the present dataset.

4.4 Limitations and future work

This study has several limitations. First, the experiments were conducted at a 1:15 Froude scale; therefore, gravity-inertia similarity was preserved, but viscous-scale effects, local turbulence through the reef openings, vortex formation around interlocking gaps, and surface-roughness effects

may not be fully reproduced. Second, the controlled wave flume environment differs from field conditions in terms of oblique and multidirectional waves, currents, seabed irregularities, biological growth, installation tolerances, and long-term environmental loading. A dedicated side-wall-effect assessment was not conducted; therefore, possible finite-width confinement effects within the 2.3-m-wide flume were not independently quantified and should be considered when extrapolating the present comparative results.

Third, the approximately 0.215-mm median sand size was not geometrically scaled, and the experiment did not focus on movable-bed similitude. The sandy profile should therefore be interpreted as a representative placement bed rather than as a quantitative prototype-scale model of scour or sediment transport; sediment mobility at model scale may differ from the prototype response. Fourth, each hydraulic scenario consisted of only one 30-min run. Statistical repeatability, confidence intervals, and run-to-run uncertainty could therefore not be quantified. Fifth, stability-state classification was observation-based, although direct observation and CCTV records were used together to improve consistency. Future experiments should include repeated runs and automated image-based tracking to quantify displacement and classification uncertainty more rigorously.

Future work should extend the experimental matrix through repeated, longer-duration runs; oblique and multidirectional wave incidence; and combined wave-current conditions. Larger-scale and field experiments are recommended to examine installation tolerances, seabed scour, long-term crown-lock durability, material degradation, and biological colonization under realistic environmental exposure. Prototype fabrication should also be evaluated using structural material requirements appropriate to the selected deployment scale. Complementary CFD or SPH modeling can resolve local flow fields, turbulence, and inter-unit hydrodynamic interactions that are difficult to observe directly, and support evaluation of configurations beyond the present laboratory matrix.

5. Conclusions

This study experimentally evaluated the hydraulic stability of interlocking and non-interlocking modular hexagonal artificial reef arrays under three prescribed irregular-wave conditions, three water levels, and seven multilayer configurations. Across the complete test matrix, the interlocking arrays achieved a mean stability of 95.5 %, compared with 72.8 % for the non-interlocking arrays, indicating higher stability for the mechanically interlocked system within the tested matrix. The benefit of interlocking became more pronounced as the prescribed hydraulic severity increased: under H15, mean stability remained 86.4 % for interlocking arrays but decreased to 51.8 % for non-interlocking arrays. Water level also influenced the response, with the LWS producing the most critical tested condition; under LWS-H15, interlocking configurations retained 50.0 - 86.4 % stability, whereas non-interlocking configurations decreased to 20.0 - 53.0 %. Stability was configuration-dependent, with 731-GR (seven-base pointy-side group configuration) showing the highest overall stability, while 631-SL (six-base flat-side single configuration) showed the greatest vulnerability among the investigated layouts. These results indicate that the crown-lock mechanism should be considered together with bottom arrangement, grouping, orientation, water level, and the designed wave condition. The dimensionless stability number is retained as a supporting system-level indicator within the adopted group-stability framework, while the paired observed unit states and percentage stability remain the primary evidence. Further validation under oblique waves, repeated runs, larger-scale or field conditions, long-term durability, and complementary numerical modeling is recommended before establishing generalized design guidance.

Acknowledgements

The authors acknowledge the support of the Department of Ocean Engineering at Institut Teknologi Sepuluh Nopember for this study. This research is funded by the Indonesian Endowment

Fund for Education (LPDP) on behalf of the Indonesian Ministry of Higher Education, Science and Technology and managed under the Enhancing Quality Education for International University Impacts and Recognition - World Class University (EQUITY) Program, under Contract No 4299/B3/DT.03.08/2025 & No 3029/PKS/ITS/2025.

Declaration of Generative AI and AI-assisted technologies

The authors used Consensus AI, Mendeley, and Grammarly to support reference enrichment and management and perform grammatical correction. With or without AI applications, the authors are fully accountable for every process of the work and manuscript writing. All final edits, interpretations, and conclusions are the sole responsibility of the authors. The authors academically and ethically confirm that the disclosure above is accurate, and the authors are ultimately responsible and accountable for the contents of the published work, including the correctness of the references in the reference list.

CRediT contribution statement

Haryo Dwito Armono: Conceptualization; Methodology; Formal Analysis, Writing - Review & Editing, Project administration; Supervision, Funding acquisition. **Suwardi**: Writing – Original Draft, Review & Editing; Investigation, Visualization; Formal analysis. **Dendy Satrio**: Methodology, Writing – Review & Editing, Resources. **Wahyudi**: Writing – Review & Editing. **Ahmad Qaedi Luthfi**: Investigation, Resources; Data Curation, Visualization.

References

Armono, H. D., Winarto, A., Sujantoko, & Ketut, S. I. (2021). A laboratory study on wave transmission over hexagonal artificial reef. *IOP Conference Series: Earth and Environmental Science*, *799*(1), 012011. https://doi.org/10.1088/1755-1315/799/1/012011

Armono, H. D., & Wirayuhanto, H. (2018). Experimental study of scouring characteristics around a hexagonal artificial reef. *MATEC Web of Conferences*, *177*, 01009. https://doi.org/10.1051/matecconf/201817701009

CIRIA, CUR, & CETMEF. (2007). *The rock manual. The use of rock in hydraulic engineering*. Ciria.

Dassanayake, D. T., & Oumeraci, H. (2012). Engineering properties of geotextile sand containers and their effect on hydraulic stability and damage development of low-crested / submerged structures. *International Journal of Ocean and Climate Systems*, *3*(3), 135-150. https://doi.org/10.1260/1759-3131.3.3.135

Dinu, I., Gràcia, V., García-León, M., Lin-Ye, J., Stănică, A., & Sánchez-Arcilla, A. (2025). Feasibility of artificial reefs as coastal protection measures at the Danube Delta coast, Romania. *Frontiers in Environmental Science*, *13*, 1568364. https://doi.org/10.3389/fenvs.2025.1568364

Eldrup, M. R., Andersen, T. L., & Burcharth, H. F. (2019). Stability of rubble mound breakwaters: A study of the notional permeability factor, based on physical model tests. *Water*, *11*(5), 934. https://doi.org/10.3390/w11050934

Elias, T., Shirlal, K. G., & E.V., K. (2021). Physical model studies on damage and stability analysis of breakwaters armoured with geotextile sand containers. *Geotextiles and Geomembranes*, *49*(3), 604-618. https://doi.org/10.1016/j.geotexmem.2020.12.001

Ghiasian, M., Carrick, J., Rhode-Barbarigos, L., Haus, B., Baker, A. C., & Lirman, D. (2021). Dissipation of wave energy by a hybrid artificial reef in a wave simulator: Implications for coastal resilience and shoreline protection. *Limnology and Oceanography: Methods*, *19*(1), 1-7. https://doi.org/10.1002/lom3.10400

Hanif, M. R., & Armono, H. D. (2022). Analisis stabilitas artificial reefs tipe hexagonal. *Rekayasa*, *15*(2), 192-198. https://doi.org/10.21107/rekayasa.v15i2.15246

Huang, J., Lowe, R. J., Ghisalberti, M., & Hansen, J. E. (2024). Wave transformation across impermeable and porous artificial reefs. *Coastal Engineering*, *189*, 104488. https://doi.org/10.1016/j.coastaleng.2024.104488

Huang, J., Lowe, R. J., Ghisalberti, M., & Hansen, J. E. (2025). Wave dissipation induced by flow interactions with porous artificial reefs. *Coastal Engineering*, *197*, 104688. https://doi.org/10.1016/j.coastaleng.2024.104688

Hughes, S. A. (1993). *Physical models and laboratory techniques in coastal engineering*. World Scientific.

Kuang, C., Ma, Y., Han, X., Pan, S., & Zhu, L. (2020). Experimental observation on beach evolution process with presence of artificial submerged sand bar and reef. *Journal of Marine Science and Engineering*, *8*(12), 1019. https://doi.org/10.3390/jmse8121019

Norris, B. K., Reguero, B. G., Bartolai, J., Yukish, M. A., Rhode-Barbarigos, L., Haus, B. K., Ojeda, G. B., Maza, M., Lara, J. L., & Beck, M. W. (2025). Designing modular, artificial reefs for both coastal defense and coral restoration. *Coastal Engineering*, *199*, 104742. https://doi.org/10.1016/j.coastaleng.2025.104742

Peng, M., Zhang, J., Zhu, Y., Gao, L., Li, S., & Pan, X. (2024). Experimental study on wave attenuation and stability of ecological dike system composed of submerged breakwater, mangrove, and dike under storm surge. *Applied Ocean Research*, *151*, 104144. https://doi.org/10.1016/j.apor.2024.104144

Ramm, L. AW., Florisson, J. H., Watts, S. L., Becker, A., & Tweedley, J. R. (2021). Artificial reefs in the Anthropocene: A review of geographical and historical trends in their design, purpose, and monitoring. *Bulletin of Marine Science*, *97*(4), 699-728. https://doi.org/10.5343/bms.2020.0046

Recio, J., & Oumeraci, H. (2007). Effect of deformations on the hydraulic stability of coastal structures made of geotextile sand containers. *Geotextiles and Geomembranes*, *25*(4-5), 278-292. https://doi.org/10.1016/j.geotexmem.2007.02.006

Recio, J., & Oumeraci, H. (2009). Process based stability formulae for coastal structures made of geotextile sand containers. *Coastal Engineering*, *56*(5-6), 632-658. https://doi.org/10.1016/j.coastaleng.2009.01.011

Suwardi, Armono, H. D., Satrio, D., Tiffany, V. K., Prakoso, A., Putro, F. L., Hanif, M. R., Erlangga, R., Khaydar, D. M., Karim, A. K., & Aswin, J. A. (2026). Artificial reefs for coastal wetland and estuary protection and coral restoration: A review. *Maritime Technology and Research*, *8*(1), 281096. https://doi.org/10.33175/mtr.2026.281096